Using measurements of the cosmic bulk flow to constrain $f(R)$ Gravity

Jacob Seiler[1,2] and David Parkinson[1]⋆

[1]*School of Mathematics and Physics, University of Queensland, Brisbane, QLD 4072, Australia*
[2]*ARC Centre of Excellence for All-Sky Astrophysics (CAASTRO), Sydney, NSW 2016, Australia*

ABSTRACT

As an alternate explanation for the cosmic acceleration, $f(R)$ theories of gravity can predict an almost identical expansion history to standard Λ cold dark matter (ΛCDM), yet make very different predictions for the growth of cosmological structures. Measurements of the cosmic bulk flow provide a method for determining the strength of gravity over the history of structure formation. We use the modified gravity N-body code ECOSMOG to simulate dark matter particles and make predictions for the bulk flow magnitude in both ΛCDM and $f(R)$ gravity. With the peculiar velocities output by ECOSMOG, we determine the bulk flow at depths ranging from 20 to $50\,h^{-1}$Mpc, following the redshift and sky distribution of the 2MASS Tully–Fisher survey (2MTF). At each depth, we find that the ΛCDM and $f_{R0} = 10^{-5}$ simulations produce bulk flow measurements that are consistent with ΛCDM predictions and the 2MTF survey at a 1σ level. We also find that adopting an $f(R)$ strength of $f_{R0} = 10^{-3}$ predict a much larger value for the bulk flow, which disagree with ΛCDM predictions at all depths considered. We conclude that f_{R0} must be constrained to a level no greater than 10^{-4} to agree with bulk flow measurements.

Key words: cosmology: theory – dark energy – large-scale structure of Universe.

1 INTRODUCTION

One of the most inescapable facts in recent cosmology is that the Universe is undergoing a period of accelerated expansion. The effect of this acceleration was observed through measurements of supernovae (Riess et al. 1998; Perlmutter et al. 1999), confirming previous indications from large-scale structure and galaxy surveys (Efstathiou, Sutherland & Maddox 1990; Krauss & Turner 1995; Ostriker & Steinhardt 1995; Yoshii & Petersen 1995). The source of this late-time acceleration has been named 'dark energy' which exerts a negative pressure to combat the attractive force of gravity.

Currently the simplest candidate for dark energy is the cosmological constant Λ. However, theoretical calculations yield a value of Λ at least 120 orders of magnitude larger than observations (Weinberg 1989; Sahni 2002). As a result, cosmological models that do not include an explicit cosmological constant form an appealing alternative. These alternatives are usually categorized depending upon which side of the Einstein equations they alter. The first category adds to or alters the energy–momentum tensor $\boldsymbol{T}_{\mu\nu}$ to yield a negative pressure (dark fluid models), while the second category alters the Einstein tensor $\boldsymbol{G}_{\mu\nu}$ to generate the acceleration (modified gravity models). Throughout this paper, we focus on a specific modified theory, $f(R)$ gravity.

$f(R)$ gravity changes the gravitational theory by modifying the action, from the standard Einstein–Hilbert action, to be some new function of the Ricci scalar R (Nojiri & Odintsov 2003; Carroll 2004). Given the freedom to choose the function $f(R)$, the expansion histories of both Λ cold dark matter (ΛCDM) and $f(R)$ models can be very similar, or even identical (Song, Hu & Sawicki 2007). Therefore, we must consider alternate methods to observationally differentiate between the models. One such approach is to study the peculiar velocity of galaxies which results from the gravitational interaction between a galaxy and the surrounding matter, causing the galaxy redshift to deviate from Hubble's Law. In essence, the peculiar velocity of a galaxy is an integrated history of its gravitational interactions, and thus provides a tool to differentiate between ΛCDM and $f(R)$ models.

Measuring peculiar velocities offers an observational difficulty as such measurements must be performed using redshift-independent distance indicators such as type Ia Supernovae (Phillips 1993), the Tully–Fisher (TF) relation (Tully & Fisher 1977) and the Fundamental Plane relation (Djorgovski & Davis 1987). A common parameter that many peculiar velocity surveys quote is the net dipole, or the 'bulk flow', of the peculiar velocity field. There has been much debate over whether the measured bulk flows are consistent with the ΛCDM model. Hong et al. (2014) analysed 2018 galaxies from the 2MASS Tully–Fisher survey (2MTF) utilizing both χ^2 and minimum variance methods, finding a bulk flow that is consistent with the ΛCDM model to a 1σ level. Conversely, Watkins, Feldman & Hudson (2009) utilized a catalogue of 4481 peculiar velocity measurements with a characteristic depth of $33\,h^{-1}$ Mpc and claim that the resulting bulk flow is inconsistent with the ΛCDM model at a >98 per cent confidence level.

⋆ E-mail: d.parkinson@uq.edu.au

A possible solution to these anomalous bulk flow measurements is to adopt a modified theory of gravity. To this end, *N*-body simulations can be employed to evolve particles under both ΛCDM and modified gravity models. The results of these simulations can then be compared to surveys such as 2MTF. An added benefit of utilizing *N*-body simulations to measure bulk flow is the lack of underlying systematic biases that most surveys are subject to. This is especially important as Keisler (2009) has shown that unaccounted systematic uncertainty could explain the discrepancies between surveys agreeing/disagreeing with the ΛCDM model.

In this paper, we utilize *N*-body simulations to measure bulk flow in both ΛCDM and $f(R)$ regimes. In Section 2, we outline $f(R)$ gravity and show how we quantify the deviation from the ΛCDM model. In Section 3, we give an overview of the simulations we use, how the output is utilized to calculate bulk flow and a brief outline of the 2MTF survey. In Section 4, we present the results of the simulations and compare them to the 2MTF survey. We conclude in Section 5.

Throughout the paper, we adopt a standard cosmology of $\Omega_m = 0.30$, $\Omega_\Lambda = 0.70$ and $H_0 = 100\,h\,\mathrm{km\,s^{-1}\,Mpc^{-1}}$. Whilst our results are h independent, we use a value of $h = 0.70$ in our simulations.

2 MODIFIED GRAVITY

Dynamics in a general relativistic regime are governed by the Einstein–Hilbert action given by

$$S = \frac{1}{16\pi G} \int d^4x \sqrt{-\mathbf{g}}\,(R + f(R)) + S_m\left(\mathbf{g}_{\mu\nu}, \Psi_m\right), \tag{1}$$

where G is the universal gravitational constant, $\mathbf{g}$ is the determinant of the metric $\mathbf{g}_{\mu\nu}$, $f(R)$ is some general function of the Ricci scalar R, S_m is the action of some matter fields Ψ_m and we have used units where $c = 1$.

By varying the action with respect to the metric, we obtain

$$\mathbf{G}_{\mu\nu} + f_R R_{\mu\nu} - \nabla_\mu \nabla_\nu f_R - \left(\frac{f(R)}{2} - \Box f_R\right)\mathbf{g}_{\mu\nu} = 8\pi G \mathbf{T}_{\mu\nu}, \tag{2}$$

where the field $f_R = \frac{\partial f(R)}{\partial R}$, $\Box = \partial^\mu \partial_\mu$ is the D'Alembert operator and $\mathbf{T}_{\mu\nu}$ is the energy–momentum tensor. If we select $f(R)$ according to ΛCDM, $f(R) = -2\Lambda$, we see that the derivatives in equation (2) vanish recovering the Einstein field equation. In the $f(R)$ regime, the *N*-body code that we use (see Section 3) employs the expression

$$f(R) = -m^2 \frac{c_1\left(-R/m^2\right)^n}{c_2\left(-R/m^2\right)^n + 1}, \tag{3}$$

where $n > 0$, c_1 and c_2 are model parameters and $m^2 = \Omega_m H_0^2$ is the characteristic length scale, with Ω_m being the present fractional matter density (Hu & Sawicki 2007).

By definition of this modified theory of gravity, there is no true cosmological constant. However, at curvatures larger than m^2, $f(R)$ may be expanded as

$$\lim_{m^2/R \to 0} f(R) \approx -\frac{c_1}{c_2}m^2 + \frac{c_1}{c_2^2}m^2\left(\frac{m^2}{R}\right)^n. \tag{4}$$

The limiting case of $\frac{c_1}{c_2^2} \to 0$, at fixed $\frac{c_1}{c_2}$, is a cosmological constant hence our model requires that as $\frac{c_1}{c_2^2} \to 0$, we approach ΛCDM

gravity. Furthermore, by taking the trace of equation (2), one obtains a field equation for f_R

$$3\Box f_R - R + f_R R - 2f(R) = -8\pi G\rho, \tag{5}$$

where ρ is the density of the Universe. As a result, the impact of $f(R)$ gravity can be viewed in terms of the field f_R (Hu & Sawicki 2007). Utilizing these two facts, we characterize the deviation from the ΛCDM model by the value of f_R at the present epoch given by

$$f_{R0} \approx -n\frac{c_1}{c_2^2}\left(\frac{12}{\Omega_m} - 9\right)^{-n-1}, \tag{6}$$

where larger n mimics ΛCDM until later times. Throughout our work, we exclusively use $n = 1$.

3 SIMULATION OUTLINE AND METHODS

3.1 Simulation outline

For all our simulations, we use 512^3 dark matter particles placed inside a box with side length $500\,h^{-1}$ Mpc. The initial conditions were generated using 2LPTIC which uses second-order Lagrangian perturbation theory thereby offering increased accuracy compared to the Zel'dovich approach (Crocce, Pueblas & Scoccimarro 2006). To specify how the 2LPTIC grid is distributed, we use the transfer function and power spectrum at $z = 0$ generated by CAMB (Lewis, Challinor & Lasenby 2000) to calculate the power spectrum at the starting redshift $z = 49$. The σ_8 value used is 0.7911 assuming a 15 per cent baryon fraction.

In this work, we use the *N*-body simulator ECOSMOG[1] which is specifically designed to simulate the universe under $f(R)$ gravity (Li et al. 2012a). ECOSMOG is based upon the RAMSES code, and uses an adaptive mesh refinement, which allows direct control of the trade-off between accuracy and speed (Teyssier 2002). We have a minimum force resolution of $0.97\,h^{-1}$ Mpc (for the course grid), increasing to a maximum of $15\,h^{-1}$kpc (with six levels of refinement), which is sufficient for our work where our minimum sphere radius is $20\,h^{-1}$ Mpc. The code works by locally solving the perturbation equations for the gravitational potential Φ and f_R field

$$\nabla^2 \Phi = \frac{16\pi G}{3}a^2\delta\rho_M + \frac{a^2}{6}\delta R(f_R), \tag{7}$$

$$\nabla^2 \delta f_R = -\frac{a^2}{3}[\delta R(f_R) + 8\pi G\delta\rho_M], \tag{8}$$

where $\delta f_R = f_R(R) - f_R(\bar{R})$, $\delta R = R - \bar{R}$, $\delta\rho_M = \rho_M - \bar{\rho}_M$ and the overbars denote the background values (Li et al. 2012a). In underdense regions, the $\delta R(f_R)$ in equation (7) vanishes causing the two equations to decouple and resulting in gravity simply being enhanced by a factor of 4/3. However, in overdense regions, δf_R becomes negligible recovering the Poisson equation for general relativity, $\delta R(f_R) = -8\pi G\delta\rho_M$.

3.2 2MTF survey

The Two Micron All-Sky Survey (2MASS; Skrutskie et al. 2006) Tully–Fisher survey (2MTF; Masters 2008) utilizes photometry data from 2MASS in conjunction with rotation and H I widths to calculate the TF distance from the redshifts in the 2MASS Redshift

---

[1] We obtained a copy of the ECOSMOG code from the authors, and used it with permission.
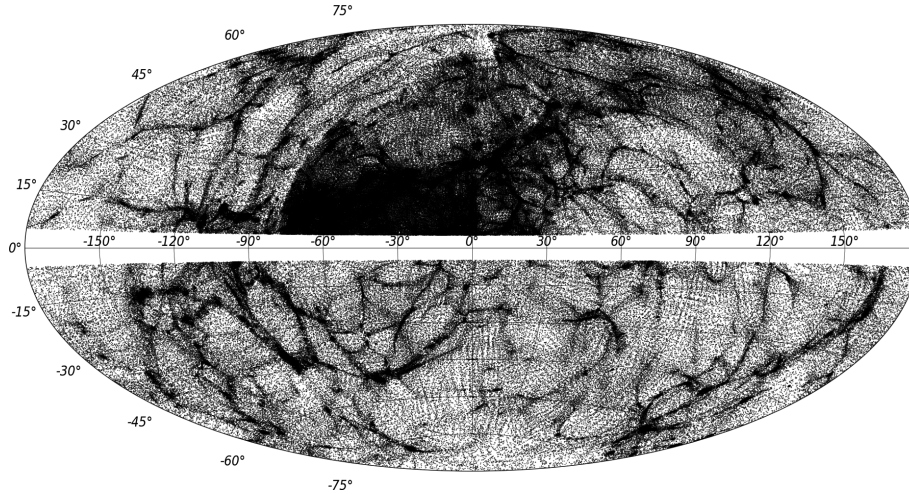
Figure 1. Aitoff projection in galactic coordinates of accepted particle positions for a single mock survey. We mimic 2MTF in that particles with latitude $|b| < 5°$ are excluded (Hong et al. 2014).

Survey (Huchra et al. 2011). In essence, 2MTF worked to calculate a universal calibration for the TF relation when utilizing the 2MASS photometry data in the *J*, *H* and *K* bands. The difficulty in deriving a global TF calibration is that thought must be given to survey specific biases as explained in depth by Masters (2008). Hong et al. (2014) then calculate peculiar velocities of 2018 galaxies by comparing the magnitude predicted by the observed redshift of the galaxy and the TF-predicted redshift.

With the peculiar velocities calculated, 2MTF determines the bulk flow at various depths by applying a χ^2 minimization using weights that account for the measurement error in distance ratio and the redshift and number density distributions of the galaxies. Hong et al. (2014) also calculates the bulk flow via other methods which we do not use for comparison in this paper for simplicity's sake.

We use the 2MTF survey as a comparison as it covers both small and large scales allowing us to probe how $f(R)$ bulk flows compare at a variety of depths. It is possible to extend our work to even larger scales utilizing other work such as Scrimgeour et al. (2016) who use data from the 6dF Galaxy Survey to calculate bulk flows of depths from 50 to 70 h^{-1} Mpc. This further comparison was not performed in this work as the data were not available at the time this research was undertaken.

3.3 Mock surveys

We run the simulation until $z = 0$ (in a comoving frame) at which point the simulator outputs the position and velocity of each dark matter particle. As the equations of motion are solved in a comoving frame, the output include only the peculiar velocity of the particle.

The bulk flow in a spherical region of radius r is given by

$$\boldsymbol{B}(r) = \frac{3}{4\pi r^3} \int\limits_{x<r} \boldsymbol{v}(\boldsymbol{x})\, \mathrm{d}^3 x, \tag{9}$$

where $\boldsymbol{v}(\boldsymbol{x})$ is the peculiar velocity field. Due to the nature of this equation, the peculiar velocity must be sampled uniformly over the volume. However, as we wish to compare our results to 2MTF in which the uniformity requirement is not met, we calculate the bulk flow via process as follows.

(i) Select a random point inside the simulation box to be the centre of the mock. This point is chosen such that any particle in the
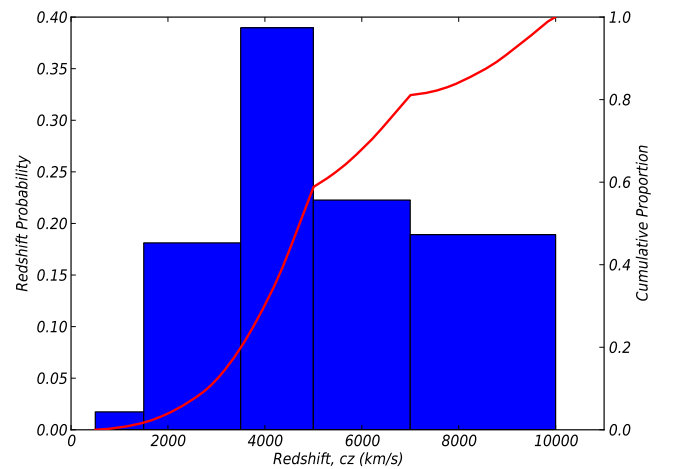

Figure 2. Mean redshift distribution (histogram left axis, cumulative proportion solid line right axis) over 50 mocks. This distribution was selected to closely follow the 2MTF survey (Hong et al. 2014).

mock survey lies within the box. For our work, we use the 2MTF distance bound of $100\,h^{-1}$ Mpc. We further select the random point such that spheres of radius $50\,h^{-1}$ Mpc will not overlap each other ensuring that each mock survey is independent.

(ii) For each particle, if it is within the distance and latitude bounds, bin the particle into the corresponding redshift bin. This redshift is the observed redshift and is calculated using equation 10, where z_{pec} is the peculiar redshift determined by projecting the peculiar velocity along the line of sight and z_{rec} is the recession redshift dictated by the comoving distance between the particle and centre of the mock. Once again we follow 2MTF which only surveyed galaxies with latitude $|b| > 5°$ (Fig. 1)

$$1 + z_{\mathrm{obs}} = (1 + z_{\mathrm{pec}})(1 + z_{\mathrm{rec}}). \tag{10}$$

(iii) Normalize the redshift histogram and create an array of accepted particles such that the resulting distribution will follow that of 2MTF (Fig. 2). The accepted particles are chosen randomly from each redshift bin. Note that the similarity between the redshift distribution of the mocks and 2MTF is not overly important and will not affect the results in a significant manner; as such, we only roughly follow the 2MTF distribution.
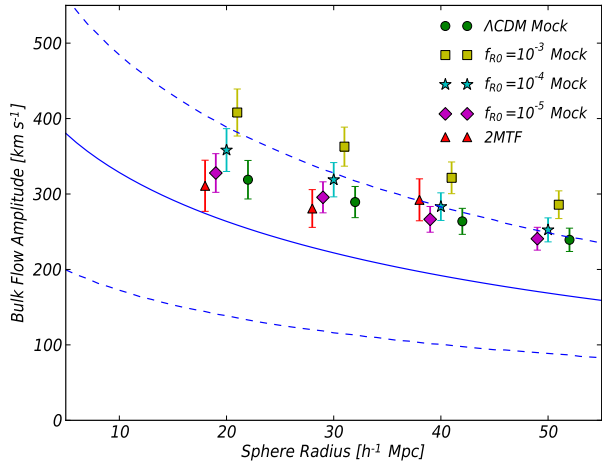
Figure 3. Average bulk flow magnitude over 50 mock surveys in ΛCDM gravity (circles), $f_{R0} = 10^{-3}$ (squares), $f_{R0} = 10^{-4}$ (stars) and $f_{R0} = 10^{-5}$ (diamonds). The error bars denote the 1σ scatter of the mocks. The solid line indicates the ΛCDM prediction with a 1σ uncertainty shown as the dashed lines. For comparison, we list the 2MTF three-band χ^2 minimization result as triangles (Hong et al. 2014). Note that the sphere radius is the same for each data set (from 20 to $50\,h^{-1}$ Mpc in intervals of $10\,h^{-1}$ Mpc) but have been shifted on this plot for better visibility.

(iv) For each sphere radius, if an accepted particle lies within the radius, add its peculiar velocity component to the total. Once all accepted particles have been checked, the bulk flow is given by equation (11) where B_x, B_y, B_z is the net peculiar velocity in each direction and N is the number of particles inside the sphere of radius r:

$$|\mathbf{B}(r)| = \frac{\sqrt{B_x^2 + B_y^2 + B_z^2}}{N}. \tag{11}$$

4 RESULTS

Fig. 3 and Table 1 show the mean bulk flow amplitude over 50 mock surveys in both ΛCDM and $f(R)$ regimes at depths ranging from 20 to $50\,h^{-1}$ Mpc. As a point of reference, we also show the 2MTF results for their three band, χ^2 minimization, at depths of 20, 30 and $40\,h^{-1}$ Mpc (Hong et al. 2014). 50 mocks provides adequate convergence for the covariance matrix for the uncertainty in the bulk flow amplitude (Appendix A2)

Following the procedure outlined in Hong et al. (2014), the ΛCDM bulk flow variance is given by

$$v_{\text{rms}}^2 = \frac{H_0^2 f^2}{2\pi^2} \int W^2 (kR) P(k)\, dk, \tag{12}$$

where H_0 is the Hubble constant, $f = \Omega_m^{0.55}$ is the linear growth rate, $W(kR) = \exp(-k^2 R^2/2)$ is the Gaussian window function, k is the wavenumber and $P(k)$ is the matter power spectrum.

The probability density function for a bulk flow amplitude B is given by

$$p(B)\,dB = \sqrt{\frac{2}{\pi}} \left(\frac{3}{v_{\text{rms}}^2}\right)^{3/2} B^2 \exp\left(-\frac{3B^2}{2v_{\text{rms}}^2}\right) dB, \tag{13}$$

where the distribution has been normalized by setting $dp(B)/dB = 0$ (Skrutskie et al. 2006). Due to the nature of bulk flow, this distribution is Maxwellian hence the peak will occur at $\sqrt{2/3}v_{\text{rms}}$. We adopt this peak as the theoretical bulk flow measurement in the ΛCDM regime with 1σ error bars given by integrating equation (13) around the peak.

From Table 1, we observe that there is little difference between ΛCDM and $f_{R0} = 10^{-5}$ bulk flow amplitudes. This is not too surprising as the $f(R)$ modification is negligible recovering standard ΛCDM. There is a noticeable increase in the bulk flow amplitude when the $f(R)$ strength is increased to $f_{R0} = 10^{-3}$ or 10^{-4}. This is the result of the Poisson equation being enhanced by the presence of a non-negligible f_R.

We find that our $f_{R0} = 10^{-5}$ and ΛCDM results agree comfortably with the 2MTF survey at all scales. Whilst the 2MTF result at $40\,h^{-1}$ Mpc agrees with all of our mocks, it disagrees with the expected trend of decreasing amplitude as sphere radius increases suggesting that we should be hesitant to take it to be as an accurate data point in comparison to our mocks. The $f_{R0} = 10^{-5}$ and ΛCDM mocks are in agreement with the theoretical predictions for all scales with the $f_{R0} = 10^{-4}$ results agreeing only at smaller scales. In essence, we are constraining f_{R0} to be below 10^{-3} and between 10^{-4} and 10^{-5} at a 1σ level. Such a constraint matches previous work where f_{R0} was constrained to $< 6 \times 10^{-5}$, $< 1.3 \times 10^{-3}$, $< 3.5 \times 10^{-3}$ and $< 1.3 \times 10^{-4}$ levels (Masters 2008; Lombriser et al. 2012a; Terukina et al. 2014; Scrimgeour et al. 2016). Furthermore, if we wished to explain the anomalous result of Watkins et al. (2009) who found a bulk flow amplitude of $407 \pm 81\,\text{km}\,\text{s}^{-1}$ (error to 3σ) on a scale of $50\,h^{-1}$ Mpc, we would need to adopt $f_{R0} > 10^{-3}$ which disagrees with both 2MTF and the previously cited work.

5 CONCLUSION

Modified gravity theories provide an appealing alternative to the ΛCDM model by providing a model that does not include an explicit cosmological constant. One such theory, $f(R)$ gravity, involves changing the Einstein–Hilbert action by altering the functional dependence upon the Ricci scalar. We consider one particular $f(R)$ model, the Hu and Sawicki model (Hu & Sawicki 2007), and parametrize the degree of deviation from the predictions of standard ΛCDM through the gradient of the function today $f_{R0} = \frac{\partial f(R)}{\partial R}|_{t=t_0}$.

The bulk flow is the net dipole moment of the cosmological peculiar velocity field, which is the result of gravitational influence on the motions of particles on large scales. As the bulk flow is sensitive to the gravitational theory considered, this results in a measurable difference in the predicted value of the bulk flow between ΛCDM and $f(R)$ gravity.

Table 1. Average flow magnitude for various gravitational models over 50 mock surveys and 2MTF survey (Hong et al. 2014). Uncertainty is given to a 1σ level and for our mocks is determined by calculating the scatter in the bulk flow amplitude.

Sphere radius (h^{-1} Mpc)	ΛCDM (km s^{-1})	$f_{R0} = 10^{-5}$ (km s^{-1})	$f_{R0} = 10^{-4}$ (km s^{-1})	$f_{R0} = 10^{-3}$ (km s^{-1})	2MTF (km s^{-1})
20	319.0 ± 25.5	327.8 ± 25.6	358.2 ± 28.4	408.0 ± 31.2	310.9 ± 33.9
30	289.3 ± 20.7	295.6 ± 20.6	319.0 ± 22.7	362.8 ± 25.9	280.8 ± 25.0
40	263.8 ± 17.3	266.4 ± 17.1	283.2 ± 18.3	321.5 ± 21.0	292.3 ± 27.8
50	239.2 ± 15.5	240.7 ± 15.1	252.5 ± 15.9	285.8 ± 18.3	–

We utilized *N*-body simulations to create a set of mock surveys under both ΛCDM and *f(R)* gravity. These mocks were analysed assuming the redshift and sky distribution of 2MTF, a previous survey that studied the bulk flow in the local Universe (Hong et al. 2014). We found that the simulations under ΛCDM and $f_{R0} = 10^{-5}$ gravity produced bulk flows that were consistent with both 2MTF and ΛCDM predictions. Choosing $f_{R0} = 10^{-4}$ gave bulk flows that agreed with the ΛCDM predictions on small scales with weak agreement on large scales. Finally, setting $f_{R0} = 10^{-3}$ resulted in bulk flows that did not agree with ΛCDM predictions to a 1σ level at all scales considered. From these results, we conclude that in order to obtain bulk flow measurements that match previous work (Masters 2008; Lombriser et al. 2012a; Dossett et al. 2014; Terukina et al. 2014; Scrimgeour et al. 2016) in addition to theoretical predictions, the upper limit on f_{R0} lies somewhere in the range 10^{-4} and 10^{-5}.

We finally note that, given the agreement between the ΛCDM and $f_{R0} = 10^{-5}$ predictions, it seems unlikely that bulk flow measurements can be of any further use in constraining the parameters in an *f(R)* theory. We have already reached the theoretical limit in which the bulk flow amplitude will provide useful information. Instead to make further progress in this area, it is more advantageous to use the full velocity power spectrum (e.g. Johnson et al. 2016).

ACKNOWLEDGEMENTS

REFERENCES

Borgani S., Da Costa L. N., Freudling W., Giovanelli R., Haynes M. P., Salzer J., Wegner G., 1997, ApJ, 282, L121
Carroll S. M., Duvvuri V., Trodden M., Turner M. S., 2004, Phys. Rev. D, 70, 043528
Crocce M., Pueblas S., Scoccimarro R., 2006, MNRAS, 373, 369
Djorgovski S., Davis M., 1987, ApJ, 313, 59
Dossett J., Hu B., Parkinson D., 2014, J. Cosmol. Astropart. Phys., 3, 46
Efstathiou G., Sutherland W. J., Maddox S. J., 1990, Nature, 348, 705
Hong T. et al., 2014, MNRAS, 445, 402
Hu W., Sawicki I., 2007, Phys. Rev. D, 76, 6
Huchra J. et al., 2011, ApJ, 199, 2
Johnson A., Blake C., Dossett J., Koda J., Parkinson D., Joudaki S., 2016, MNRAS, 458, 3
Keisler R., 2009, ApJ, 707, L42
Krauss L. M., Turner M. S., 1995, Gen. Relativ. Gravit., 27, 1137
Lewis A., Challinor A., Lasenby A., 2000, ApJ, 538, 473
Li B., Zhao G., Teyssier R., Koyama K., 2012a, J. Cosmol. Astropart. Phys., 1, 051
Li J., Newberg H. J., Carlin J. L., Deng L., Newby M., Willett B. A., Xu Y., Luo Z., 2012b, ApJ, 757, 151
Lombriser L., Schmidt F., Baldauf T., Mandelbaum R., Seljak U., Smith R.E., 2012a, Phys. Rev. D., 85, 10
Lombriser L., Slosar A., Seljak U., Hu W., 2012b, Phys. Rev. D, 85, 12
Masters K., Springob C. M., Huchra J. P., 2008, AJ, 135, 1738
Nojiri S., Odintsov S. D., 2003, Phys. Rev. D, 68, 123512
Ostriker J. P., Steinhardt P. J., 1995, Nature, 377, 600
Perlmutter S. et al., 1999, ApJ, 517, 565
Phillips M. M., 1993, ApJ, 413, L105
Ries A. G. et al., 1998, ApJ, 116, 1009
Sahni V., 2002, Class. Quant. Grav., 19, 3435
Scrimgeour M. et al., 2016, MNRAS, 455, 386
Skrutskie M. et al., 2006, AJ, 131, 1163
Song Y. S., Hu W., Sawicki I., 2007, Phys. Rev. D, 75, 044004
Terukina A., Lombriser L., Yamamoto K., Bacon D., Koyama K., Nichol R. C., 2014, J. Cosmol. Astropart. Phys., 04, 013
Teyssier R., 2002, A&A, 385, 337
Tully R. B., Fisher J. R., 1977, A&A, 54, 661
Watkins R., Feldman H. A., Hudson M. J., 2009, MNRAS, 392, 743
Weinberg S., 1989, Rev. Mod. Phys., 61, 1
Yoshii Y., Peterson B. A., 1995, ApJ, 444, 15

APPENDIX A

A1 Line of sight vs 3D velocity

Throughout most of the literature, authors simply state that the bulk flow in 1D is a factor of $1/\sqrt{3}$ smaller than the full 3D amplitude (Watkins et al. 2009; Huchra et al. 2011). However, the reasoning behind this factor is not fully explored. In this appendix, we wish to briefly give an overview of the logic behind the $1/\sqrt{3}$ factor difference between line of sight and 3D bulk flow amplitude.

Consider particles with velocity $\boldsymbol{v}_{3D} = (v_x, v_y, v_z)$. We choose to position our coordinate system such that one of the axes lies precisely along the line of sight yielding a velocity $\boldsymbol{v}_{LoS} = v_x$. Then, the ratio of the 3D and the line-of-sight bulk flows in such a situation is given by

$$\frac{\boldsymbol{B}_{3D}(r)}{\boldsymbol{B}_{LoS}(r)} = \sqrt{\frac{v_x^2 + v_y^2 + v_z^2}{v_x^2}}, \tag{A1}$$

$$= \sqrt{1 + \frac{v_y^2 + v_z^2}{v_x^2}}. \tag{A2}$$

These velocities are drawn from a Maxwellian distribution with the same variance. In Fig. A1, we plot a histogram of 10 000 ratios following equation (A2). We see that the peak of this distribution is centred on $\sqrt{3}$ despite the arithmetic mean occurring at a higher
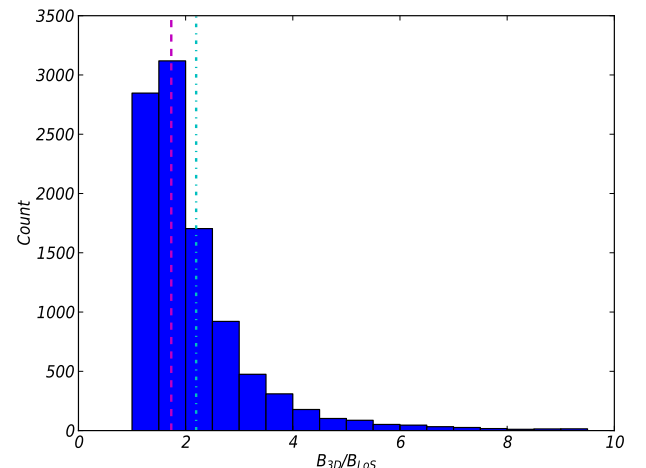

Figure A1. Distribution for the ratio between 3D and line-of-sight bulk flows. The dashed line is at $\sqrt{3}$ which matches literature and the dash–dotted line depicts the arithmetic mean of the distribution with a value of 2.19.
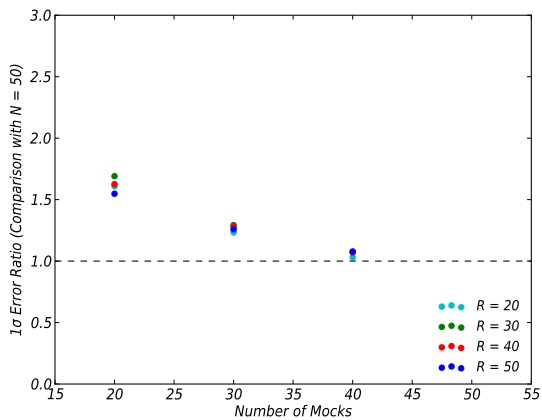
Figure A2. Ratio of the 1σ uncertainty in the bulk flow amplitude for the ΛCDM simulation (with reference to $N = 50$ mocks) for different radii (in units of h^{-1} Mpc).

value of 2.19. This is due to $v_x \ll v_y$, v_z case skewing the ratio towards extremely high values. Thus, the 1D amplitude of the bulk flow is not the arithmetic mean of the individual particle contributions (as might be assumed), but rather the peak of the distribution.

A2 Uncertainty convergence

In this appendix, we show that the number of mocks ($N = 50$) provides adequate convergence for the uncertainty in the bulk flow amplitudes. We do this by varying the number of mocks from 10 to 50 and plotting the ratio of the 1σ uncertainty (with reference to $N = 50$ mocks) in Fig. A2. We see that as the number of mocks approaches 50 we approach convergence, and this is true for every sphere radius.

This paper has been typeset from a T$_{\rm E}$X/L$^{\rm A}$T$_{\rm E}$X file prepared by the author.